 doi:10.20944/preprints202204.0023.v1

Article

A hybrid self-seeded Ti:sapphire laser with a pumping scheme based on spectral beam combination of continuous-wave diode and pulsed DPSS lasers

Volker Sonnenschein [1,*] and Hideki Tomita [1]

[1] Department of Energy Engineering, University of Nagoya, Japan
* Correspondence: sonnevolker@gmail.com

Abstract: A wide variety of applications require high peak laser intensity in conjunction with a narrow spectral linewidth. Typically, injection-locked amplifiers have been employed for this purpose, where a continuous wave oscillator is amplified in a secondary external resonant amplifier cavity using a pulsed pump laser. In contrast, here we demonstrate a setup that combines a CW Ti:sapphire oscillator and pulsed amplifier in a single optical cavity, resulting in a compact system. Dichroic beam combination of blue wavelength semiconductor diodes and the green wavelength of a Nd:YAG laser allowed the simultaneous excitation of the Ti:sapphire crystal by both continuous-wave and pulsed pump sources. A linewidth of <2 MHz is achieved in continuous wave operation, while the linewidth increases to about 10 MHz in the combined CW + pulsed mode with a pulse duration of 73 ns. A peak pulse intensity of 0.2 kW is achieved, which should enable efficient single-pass second harmonic generation in a nonlinear crystal.

Keywords: Ti:sapphire laser, amplifier, injection-lock, Diode pumping, solid state laser

1. Introduction

A combination of a low power laser oscillator (often referred to as 'seed' or 'master' laser) and external amplifier is widely used to increase the intensity of a laser beam, while retaining important characteristics of the oscillator. Depending on applications these characteristics can be either wavelength and linewidth, pulse envelope, other parameters such as beam profile and polarization or any combination thereof. For low gain media, such as Titanium:sapphire (Ti:sa), a single-pass amplifying stage is usually insufficient, so that a resonant or regenerative amplifier stage is more practical. If a narrow spectral linewidth and precise transfer of the wavelength from seed to amplifier output is desired, the laser frequency of the seed needs to be at least partially stabilized to a longitudinal mode of the amplifier cavity or vice versa.

Such pulsed narrow linewidth laser sources are desired in many types of atomic and molecular spectroscopic techniques such as laser cooling of antihydrogen [1], measurements of the size of the proton in muonic hydrogen and helium[2][3] or high resolution resonance ionization spectroscopy for high precision measurements of isotope shifts or hyperfine structure in exotic nuclei. To reduce line-broadening effects Doppler-free two-photon excitation [4][5], supersonic gas jets [6][7][8] or cross-beam geometries [9][10][11] have been used. Often a high power laser can even be detrimental in these applications, as power broadening of transition lines may increase the measurement uncertainty. However, many atomic and molecular absorption lines lie in the UV or mid-to-far infrared, not directly accessible with many laser sources. Conversion to these wavelength regions by nonlinear processes in crystals or other nonlinear media requires high laser intensities, especially if convenient single-pass frequency conversion is to be used. Several injection-locked Ti:sapphire amplifiers have been developed for remote water vapor sensing using differential absorption lidar (DIAL)[12][13][14]. Other applications include four-wave-mixing [15] as well as coherent Raman spectroscopy and microscopy [16] [17][18]. Further benefits of Injection seeding relevant in these cases are a reduction in timing jitter and intensity fluctuations [19].

 doi:10.20944/preprints202204.0023.v1

In practice the implementation of these laser sources requires two laser cavities and two feedback loops for wavelength control. One loop to stabilize the frequency of the oscillator itself and another to lock the amplifier to the oscillator, also referred to as 'injection-lock'. Injection locking techniques are possible both for continuous wave (CW) as well as pulsed amplifiers. For CW amplifiers the error-signal required to establish the feedback loop is typically generated via modulation and phase-sensitive detection. Dithering of the cavity with piezo actuators or higher bandwidth techniques such as Pound-Drever-Hall[20] with electro- or acousto-optic modulators are widely used for this. In pulsed amplifiers the high peak intensity during the pulse can often saturate the photo-detectors used to sample the CW signal and add noise to the system. To circumvent this, additional optical or electronic circuitry to blank the signal during the pulse are often applied[21] or alternative locking schemes, such as 'ramp-hold-fire' [22][23] or minimization of pulse build-up time [24] can be employed.

The need for two separate laser cavities naturally has disadvantages due to the increased complexity, cost and space requirements. Direct generation of narrow-linewidth radiation from a single pulsed laser cavity however is difficult, as each individual laser pulse builds up from an effectively random distribution of photons, so that strong line narrowing via multiple frequency-selective intracavity elements such as etalons, birefringent filters, prisms or gratings is needed. Even if doing so, a truly longitudinal single-mode operation with controllable mode-hop free wavelength tuning is very difficult to achieve. Furthermore, the additional intracavity losses will limit the efficiency of the system, while the high pulse intensity may cause optical damage on the tuning elements.

Techniques such as self-seeding, self-injection as well as prelasing of pulsed lasers have been attempted to achieve these goals with reduced losses. In self-seeded lasers [25][26][27] either a portion of the laser is re-injected into the cavity by an external reflector or a coupled dual-cavity configuration with either a single or multiple gain media is used. One cavity features strong frequency selection, but low gain and power to generate a narrow linewidth seed. This seed couples via a partially reflective surface or via electro-optic switching [28] to a lower loss and less selective cavity. In this way, portions of the same cavity or even the same gain medium can be used both for generation of the seed as well as for amplification. With a grazing incidence grating configuration single longitudinal mode operation has been achieved [29] even enabling wavelength scanning and control using a scheme based on monitoring angular deviations of the laser output [30]. Drawbacks of these approaches are the typically low efficiency and high lasing threshold of grazing incidence cavities as well as a fairly complex and slow feedback scheme using either CCD sensors or segmented photodiodes, resulting in a relatively large pulse-to-pulse frequency jitter of 40 MHz[31]. Nevertheless, this is a promising technique for moderate-resolution spectroscopy. In a similar manner, prelasing[32][33][34] uses a scheme where the cavity is at first kept at low round-trip gain, until the linewidth has sufficiently decreased, at which point the pump intensity is increased or the loss is reduced to generate a strong output pulse.

The method and system described in this paper is most comparable with pre-lasing, however as the pre-lasing here is performed without interruptions, a continuous error signal for wavelength stabilization and control can be generated and mode-hop free frequency tuning is made feasible. In addition, our system combines CW semiconductor diode laser pumping with a pulsed high power diode pumped solid state (DPSS) pump, taking advantage of recent advances in high power blue diode laser manufacturing and easy beam combination via dichroic mirrors. There has been rapid progress in the development of diode pumped Ti:sapphire lasers with availability of low-priced high power diodes. First commercial Ti:sapphire systems based on this technology have been introduced. Much of the recent research focus has been on the development of diode-pumped mode-locked oscillators [35][36][37][38], with a recent review [39] summarizing many of the developments. Though some work has been done in characterizing CW operation [40][41][42], we are only aware of our groups own system featuring single-frequency CW operation[43][44] of a diode-pumped Ti:sapphire laser.

Preprints (www.preprints.org) | NOT PEER-REVIEWED | Posted: 5 April 2022 doi:10.20944/preprints202204.0023.v1

The beam quality of high power visible diode lasers in the blue-green wavelength region is fairly poor. However, a tight focusing geometry combined with a short, highly-doped Ti:sapphire crystal can reach sufficient gain to enable continuous wave Ti:sapphire laser operation with several intracavity elements as we have demonstrated in our previous prototype. Though there are some changes in the geometry of the laser cavity presented here, the general operating principle is similar. Compared to the four pump diodes (two blue, two green) used in the earlier prototype, only two blue diodes were used here, limiting the wavelength tuning range to about 730-855 nm.

2. Materials and Methods

2.1. Laser setup

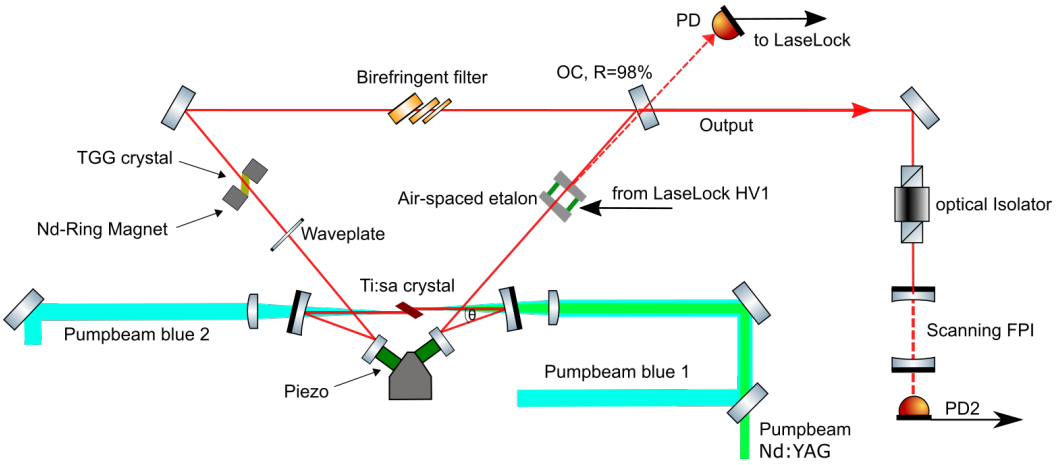

Figure 1. Optical layout of the laser system.

A schematic of the experimental setup is displayed in Figure 1. Two blue multimode pump diodes (NUBM07E, 465 nm) were each collimated with a f= 4.2 mm aspheric lens and shaped by a single cylindrical lens telescope by vertical stacking (not shown). Two additional green diodes were usually used with the system, but their beam transport path was blocked for the purposes of this experiment. One of the blue diodes was overlapped with the second harmonic output (532 nm) of a pulsed Nd:YAG laser (Edgewave BX-611e) using a dichroic mirror. According to manufacturer specifications, this pulsed laser has a minimum pulse duration of 1 ns, high beam quality with $M^2 = 1.1$ and a maximum pulse repetition rate (PRR) of 100 kHz. During first tests the counter-propagating blue diode was damaged by the remaining transmission of the YAG through the crystal, even while using one dichroic mirror for green wavelength rejection in its path. So after replacement, one additional dichroic filter was installed to protect it. We assume that even after considering 90% absorption in the Ti:sapphire crystal, a separation ratio of $> 1/1000$ is required for safe operation due to the high peak intensity of the YAG laser. Both diodes and the Nd:YAG laser were focused into the Ti:sapphire crystal using f= 60 mm achromatic lenses.

The folded bow-tie cavity uses a 4 mm thick Brewster-cut Ti:sapphire crystal (GT Advanced technologies, FOM = 150). Curved mirrors with a radius of curvature of 75 mm are positioned at an angle of incidence of 8 degrees to compensate the astigmatism introduced by the crystal. As the acute angle of reflection would necessitate a very long-stretched cavity geometry to accommodate other optical mounts, two folding mirrors attached to piezo actuators pick up the laser light close to their edge and redirect the beam. To achieve unidirectional emission from the ring-laser an optical diode based on a 3 mm thick TGG crystal placed in a cylindrical Neodymium ring magnet and an adjustable $\lambda/2$ waveplate are installed. Frequency selection is performed with a three-plate birefringent filter (Sirah Lasertechnik) and self-made etalon(R= 4%, FSR $\approx$ 18 GHz). Assembly of the air-spaced etalon was performed by aligning two single-side AR-coated wedged windows inside a laser cavity and gluing them onto a ring piezo actuator so that the uncoated sides were

 doi:10.20944/preprints202204.0023.v1

parallel to each other. Cavity mirrors were HR-coated for 700-950 nm at 0-20° AOI (R=99.9% and T >0.05%) and highly transmissive for 460-520 nm. An output coupler (OC) with T=2% from 700-900 nm was used. While this OC does not maximize the output efficiency of the system, it allowed for a wide wavelength tuning range of > 160 nm in CW mode, if using all four pump diodes.

2.2. Operation and stabilization

The two pump diodes, each operating at an average power of about 1.8 W, keep the laser operating just above lasing threshold at all times. This CW signal is monitored by reflecting a fraction of the light from the surface of the etalon to an amplified photodiode. Dithering of the length of the etalon by applying a sinusoidal modulation voltage and lock-in detection of the induced intensity fluctuations generates an error signal. This signal is proportional to the frequency mismatch between laser cavity mode and etalon mode and can be used to synchronize the etalon to changes of the cavity mode, thus preventing mode-hops. The narrowband CW Ti:sa laser light is then amplified after the Nd:YAG pump pulse is applied. While the pulsed pump source introduced a considerable source of noise to the error signal used for wavelength stabilization, suitable conditions for stable operation and wavelength scanning were determined.

Control of the Piezo actuator voltages, as well as generation of modulation signal, filtering and PID control is done using a commercial servo controller (TEM Laselock), which features two independent regulators. Internally, the Laselock first digitizes the photodiode signal, mixes it with the oscillating dither voltage and performs low-pass filtering to generate the error signal. This error signal is then amplified according to the PID controller settings and fed back to the HV output controlling the etalon piezo.

3. Results

3.1. Error signals and Locking performance

To maximize the signal-to-noise (SN) ratio of the error signal in the hybrid CW+pulsed mode, the gain of the PD amplifier was adjusted to keep the CW signal slightly below the maximum input level of the Laselock (1 V). During the pulses the detected signal reached the saturation limit of the detector (5 V), so that the input signal was clipped, reducing the amount of noise introduced. Furthermore, the dither amplitude was increased by a factor of four compared to our usual CW operating settings. In the Laselock system the dither amplitude is given as a percent value of the maximum voltage range (150 V) and a value of 0.2% or 0.3 V was used in the experiment. The phase of the lock-in detection was set to 90°degree and the frequency of the dither was tuned to a mechanical resonance of the piezo assembly at about 147 kHz where the error signal was maximized. At dither frequencies close to a multiple of the PRR of the Nd:YAG laser significant additional noise was observed.

The system was first operated with CW pumping only. When ramping the etalon piezo-voltage with PID control turned off, a clean error signal is observed as shown in Figure 2. Here the error signal has clean linearly increasing sections, separated by jumps during mode-hops of the laser frequency. The zero-crossing point of the error signal (indicated with dashed horizontal and vertical lines) coincides with minimal intensity fluctuations in the photodiode signal, indicating that the etalon transmission peak matches to the frequency of a cavity mode. Turning the piezo ramp off and activating the PID loop results in the data in Figure 3, where the error signal stays close to zero and the PD signal is stable.

Finally, when introducing the pulsed pumping, the situation changes as shown in Figures 4 and 5. Though the PD signal now fluctuates wildly, the error signal during the piezo ramp still shows linear trends separated by mode-hops, though with significant addition of noise. In the locked state the error signal varies much more compared to the CW mode, but the amplitude of the fluctuations still stays within a smaller range than in

Preprints (www.preprints.org) | NOT PEER-REVIEWED | Posted: 5 April 2022 doi:10.20944/preprints202204.0023.v1

scanned mode, so that it can be assumed that no mode-hops occur. We note that this noise only weakly scaled with pulse energy, so that this effect did not restrict power scaling.

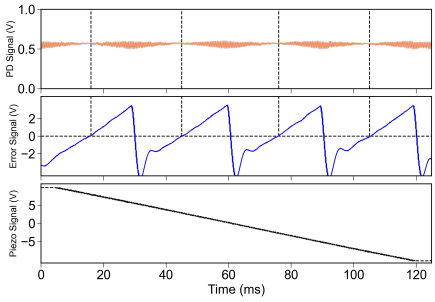

Figure 2. PD and error signals in CW-only mode - scanning.

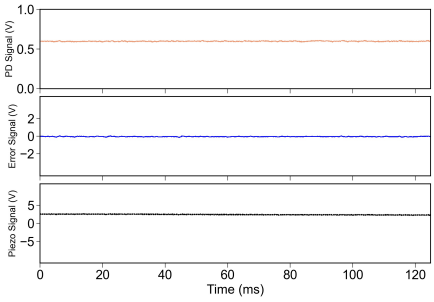

Figure 3. PD and error signals in CW-only mode - locked.

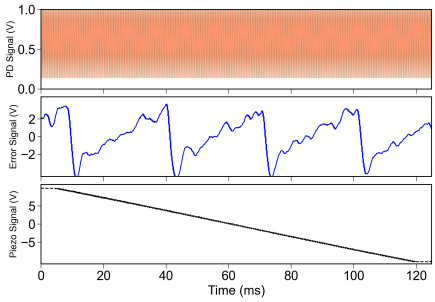

Figure 4. PD and error signals in CW+pulsed mode - scanning.

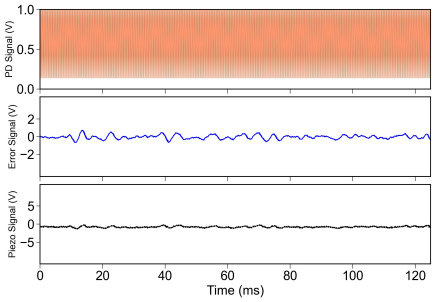

Figure 5. PD and error signals in CW+pulsed mode - locked.

3.2. Output power and efficiency

The pump diodes were set to a power level to reach about 20 mW of CW output power. It was noticed that the optimum position of the achromatic pump lens was slightly different for the diode pump and the Nd:YAG laser. To maximize the achieved pulse energy the pump lens position was optimized for the Nd:YAG laser and the power of the diodes was increased to compensate for the loss in CW power. The wavelength was fixed at 790 nm close to the gain peak of Ti:sapphire. A thermal power-meter was used to measure the average power of both the pump laser and the Ti:sapphire laser output. To estimate the output pulse energy as shown in Figure 6 the average power was divided by the PRR after subtracting the CW baseline. This may cause a slight underestimate of the true pulse energy, as the pulsing causes a short-term depletion of the inversion after the pulse, meaning that the average CW baseline would be reduced in the CW+pulsed mode.

The pulse energy conversion efficiency dropped from about 10% at low pump energy to about 7% at our highest setting. This reduction of efficiency was also observed in the absence of CW pumping and is still unexplained. At a pump energy of 95 μJ the output pulse shape was measured using a PD with 50 MHz bandwidth (Thorlabs PDA8A2), displayed in Figure 7, yielding a FWHM pulse duration of 73(5) ns, not corrected for the PD impulse response function. Assuming that the true pulse duration is shorter than this value, a peak power of about $E/\Delta T = 15.4\,\mu J/73\,ns = 0.21$ kW is reached at maximum pump energy.

3.3. Linewidth measurement

To measure the spectral linewidth of the pulsed laser, the output was sent via an optical isolator to a scanning FPI (Toptica FPI 100) with a specified FSR of 1 GHz. A scan

Preprints (www.preprints.org) | NOT PEER-REVIEWED | Posted: 5 April 2022 doi:10.20944/preprints202204.0023.v1

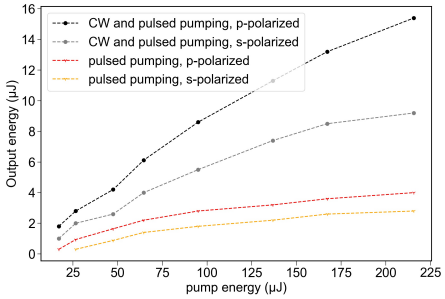

Figure 6. Ti:sapphire laser pulse energy as a function of pump pulse energy.

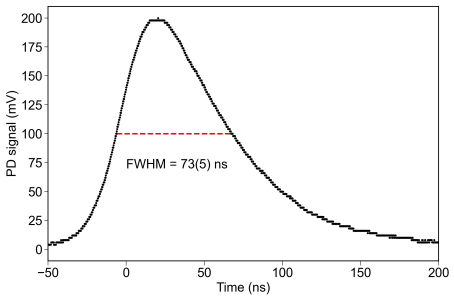

Figure 7. FWHM Pulse duration of the Ti:sapphire output.

generator applied a saw-tooth voltage ramp to the FPI piezo covering a scan-range of about two FSR. As seen in figure 8, a fairly slow scan was performed and the delay between two succeeding transmission peaks was measured. Following this, a single transmission peak was observed in higher resolution as revealed in the inset. The peak consists of several short pulses spaced according to the PRR of 5 kHz of the laser. The signal amplitude at each point in time is the overlap of the spectral distribution of the Ti:sapphire laser pulse with the Airy transmission peak of the interferometer. From the shape of the envelope of pulses the spectral distribution can be assumed to be approximately Gaussian. Additionally, as the pulse-to-pulse amplitude fluctuations are small, the pulse-to-pulse frequency jitter must be smaller than the linewidth. Based on the ratio of the FSR to the FWHM of the pulse envelope a linewidth of 11(3) MHz is estimated, with the error dominated by the unmeasured nonlinear expansion of the piezo actuator in the FPI. Typically a relative nonlinearity of $< 20\%$ can be assumed for common piezo materials.

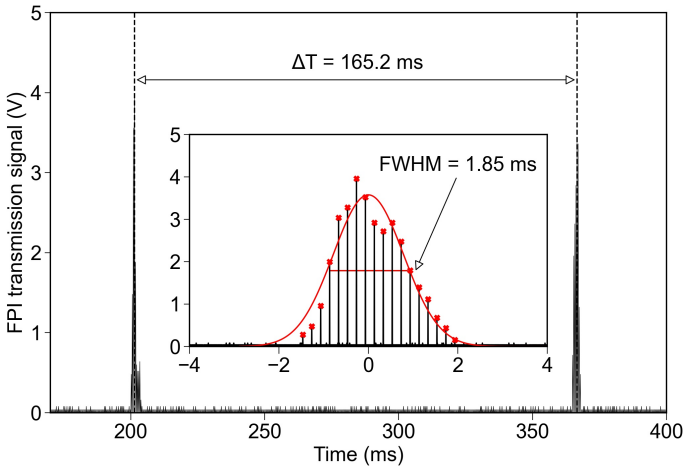

Figure 8. Transmission fringes of the FPI. Due to the pulsed operation a slow scan was performed, so that each transmission peak contained several pulses, allowing a fit of the peak envelope as shown in the inset.

3.4. Frequency scanning

The laser light leaking through one of the cavity's HR mirrors was coupled into an optical fiber for analysis by a wavemeter (HighFinesse WS6-600). The etalon was locked and a slow triangle voltage ramp was applied to the Piezo-mounted mirrors of the cavity. The wavelength change over time was recorded in both CW and CW+pulsed mode, shown in Figure 9. No significant change of behavior between the two operating modes could be observed within the resolution of the wavemeter and no mode-hops occurred. The

Preprints (www.preprints.org) | NOT PEER-REVIEWED | Posted: 5 April 2022 doi:10.20944/preprints202204.0023.v1

tuning range of 12 GHz shown here was slightly smaller than the present limit of 17 GHz set by the piezo actuator range. For tuning ranges of >12 GHz sometimes mode-hops occurred, which may be avoided by adding a thin etalon to the cavity, or synchronizing the birefringent filter rotation with the etalon scan. The wavelength change was not perfectly linear due to the piezo hysteresis and had some slight perturbations. As the cavity had no enclosure, these were likely caused by airflow or pressure changes.

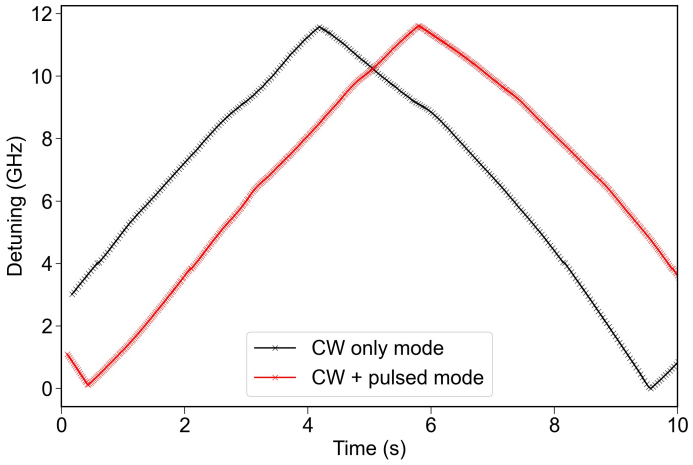

Figure 9. Slow frequency scan of the Ti:sapphire laser showing mode-hop free operation in CW and pulsed mode.

4. Discussion and Conclusion

A self-seeded hybrid CW and pulsed Ti:sapphire laser system has been developed. Compared to other pulsed self-seeded or pre-lasing approaches the present system allows precise and mode-hop free control of the laser frequency using only minor modifications to standard techniques typically used in many CW laser systems. The pulsed gain modulation of the cavity caused significant noise in the error signal for regulation, however for a PRR below 10 kHz this was found to be not prohibitive for stable operation. Use of an electrooptic etalon [45] to achieve higher dither frequencies may help in improving the SN ratios to allow operation at higher PRR.

Analysis of the spectral linewidth and monitoring via a commercial wavemeter provides evidence that the system should be suitable for high resolution spectroscopy, such as required for studies of hyperfine structure and isotope shifts. The linewidth was found to be about 11 MHz, which is comparable to the natural linewidth of many optical dipole transitions in atoms and molecules and is only slightly larger than the Fourier transform limit expected for the measured pulse duration of 73(5) ns.

The present laser cavity exhibited fairly high intracavity losses and has a small output-coupling ratio of 2%, which limited efficient energy extraction. High intracavity-losses are typical for diode pumping of Ti:Sapphire lasers, as the high crystal doping concentrations required are correlated with a poor FOM value[46][47] indicating high self-absorption at the lasing wavelength. If a narrower wavelength tuning range is sufficient a higher output coupling ratio can be used, which should significantly improve efficiency. Furthermore, no efforts to optimize the mode-matching of the pulsed pump laser to the cavity mode were made, so additional performance gains are anticipated here. Specifically, the Nd:YAG mode diameter in front of the pump lens was about 4 mm, resulting in a Rayleigh range of only about 0.15 mm based on calculations, which is much shorter than the crystal length.

Due to the fairly small Ti:sapphire mode diameter in the laser crystal, scaling to much higher pulse energies is not feasible with the present design because of gain saturation and optical damage thresholds. This could be alleviated using a two-crystal cavity, were one

 doi:10.20944/preprints202204.0023.v1

highly doped crystal is used for CW pumping and another weakly-doped, high FOM crystal is placed at a different cavity location for pulsed pumping. This also would effectively eliminate concerns of damaging the CW diodes with the pulsed pump laser as their optical paths would be separated. In this case nothing impedes the use of additional green CW diode pumping anymore, increasing the maximum CW gain. Thus, the cavity could be optimized for either wider tuning range or increased extraction efficiency. Alternatively, steep-edge dichroic filters may be used to separate the green diode wavelengths (520-525 nm) from the Nd:YAG wavelength (532nm).

A different option to achieve higher performance would the inclusion of intracavity second harmonic generation [48][49][50]. This would allow the use of a HR mirror for the fundamental wavelength instead of the OC, resulting in a lower CW lasing threshold, but at the same time enabling higher nonlinear output coupling during the pulse peak via the SHG process. Based on the output peak power of 0.2 kW the circulating intracavity peak power should approach up to 10 kW, potentially yielding very high conversion efficiency. A secondary focus in the cavity for the SHG crystal may be advantageous in this case.

In conclusion, our system provides narrow linewidth at medium power levels, sufficient for many applications. The system balances between the complexity and cost of typical injection-locked Ti:sapphire laser systems and pure pulsed systems, which usually exhibit poorer spectral purity and linewidth. Various improvements to further increase efficiency and performance of the laser are envisaged to make it more competitive with existing solutions.

Funding: This work was partially supported by JSPS Grant-in-Aid for Scientific Research 19H05584, the Japan Science and Technology Agency (JST) PRESTO Grant Number JPMJPR19G7 and JST SCORE University Promotion Type (Developing the Environment for Creation of Startup Ecosystem in Startup Cities Type), Grant Number JPMJST2076.

Institutional Review Board Statement: "Not applicable"

Acknowledgments:

Conflicts of Interest: "The authors declare no conflict of interest."

Abbreviations

The following abbreviations are used in this manuscript:

CW	continuous wave
DPSS	Diode-pumped Solid-state
FOM	Figure of Merit
FPI	Fabry Pérot Interferometer
FSR	Free Spectral Range
FWHM	Full Width at Half Maximum
HR	High Reflector
HV	High Voltage
Nd:YAG	neodymium-doped yttrium aluminum garnet
OC	Output Coupler
PD	Photodiode
PID	Proportional-Integral-Derivative
PRR	pulse repetition rate
SHG	second harmonic generation
SN	signal-to-noise
TGG	Terbium Gallium Garnet
Ti:sapphire	titanium-doped sapphire

References

1. Gabrielse, G.; Glowacz, B.; Grzonka, D.; Hamley, C.D.; Hessels, E.A.; Jones, N.; Khatri, G.; Lee, S.A.; Meisenhelder, C.; Morrison, T.; et al. Lyman-α source for laser cooling antihydrogen. *Opt. Lett.* **2018**, *43*, 2905–2908. doi:10.1364/OL.43.002905.

2. Pohl, R.; Antognini, A.; Nez, F.; Amaro, F.D.; Biraben, F.; Cardoso, J.M.R.; Covita, D.S.; Dax, A.; Dhawan, S.; Fernandes, L.M.P.; et al. The size of the proton. *Nature* **2010**, *466*, 213–216. doi:10.1038/nature09250.
3. Krauth, J.J.; Schuhmann, K.; Ahmed, M.A.; Amaro, F.D.; Amaro, P.; Biraben, F.; Chen, T.L.; Covita, D.S.; Dax, A.J.; Diepold, M.; et al. Measuring the α-particle charge radius with muonic helium-4 ions. *Nature* **2021**, *589*, 527–531. doi:10.1038/s41586-021-03183-1.
4. Wendt, K.; Mattolat, C.; Gottwald, T.; Kron, T.; Raeder, S.; Rothe, S.; Schwellnus, F.; Tomita, H. Hyperfine structure and isotope shift in the $3s^2\ 3p^2\ ^3P_{0,1,2} \rightarrow 3s^2\ 3p4p\ ^3P_{0,1,2}$ transitions in silicon by Doppler-free in-source two-photon resonance-ionization spectroscopy. *Phys. Rev. A* **2013**, *88*, 052510.
5. Chrysalidis, K.; Wilkins, S.; Heinke, R.; Koszorus, A.; De Groote, R.; Fedosseev, V.; Marsh, B.; Rothe, S.; Garcia Ruiz, R.; Studer, D.; et al. First demonstration of Doppler-free 2-photon in-source laser spectroscopy at the ISOLDE-RILIS. *Nuclear Instruments and Methods in Physics Research Section B: Beam Interactions with Materials and Atoms* **2020**, *463*, 476–481. doi:10.1016/j.nimb.2019.04.020.
6. Ferrer, R.; Barzakh, A.; Bastin, B.; Beerwerth, R.; Block, M.; Creemers, P.; Grawe, H.; de Groote, R.; Delahaye, P.; Fléchard, X.; et al. Towards high-resolution laser ionization spectroscopy of the heaviest elements in supersonic gas jet expansion. *Nature Communications* **2017**, *8*, 14520. doi:10.1038/ncomms14520.
7. Granados, C.; Creemers, P.; Ferrer, R.; Gaffney, L.P.; Gins, W.; de Groote, R.; Huyse, M.; Kudryavtsev, Y.; Martínez, Y.; Raeder, S.; et al. In-gas laser ionization and spectroscopy of actinium isotopes near the $N = 126$ closed shell. *Phys. Rev. C* **2017**, *96*, 054331. doi:10.1103/PhysRevC.96.054331.
8. Ferrer, R.; Verlinde, M.; Verstraelen, E.; Claessens, A.; Huyse, M.; Kraemer, S.; Kudryavtsev, Y.; Romans, J.; Van den Bergh, P.; Van Duppen, P.; et al. Hypersonic nozzle for laser-spectroscopy studies at 17 K characterized by resonance-ionization-spectroscopy-based flow mapping. *Phys. Rev. Research* **2021**, *3*, 043041. doi:10.1103/PhysRevResearch.3.043041.
9. Sonnenschein, V.; Moore, I.D.; Raeder, S.; Reponen, M.; Tomita, H.; Wendt, K. Characterization of a pulsed injection-locked Ti:sapphire laser and its application to high resolution resonance ionization spectroscopy of copper. *Laser Physics* **2017**, *27*, 085701. doi:10.1088/1555-6611/aa7834.
10. Studer, D.; Ulrich, J.; Braccini, S.; Carzaniga, T.S.; Dressler, R.; Eberhardt, K.; Heinke, R.; Köster, U.; Raeder, S.; Wendt, K. High-resolution laser resonance ionization spectroscopy of $^{143-147}$Pm. *The European Physical Journal A* **2020**, *56*, 69. doi:10.1140/epja/s10050-020-00061-8.
11. Kessler, T.; Tomita, H.; Mattolat, C.; Raeder, S.; Wendt, K. An injection-seeded high-repetition rate Ti:Sapphire laser for high-resolution spectroscopy and trace analysis of rare isotopes. *Laser Physics* **2008**, *18*, 842. doi:10.1134/S1054660X08070074.
12. Metzendorf, S. 10 W-Average-Power single-frequency Ti:sapphire Laser with tuning agility – A breakthrough in high-resolution 3D water-vapor measurement. PhD thesis, Universität Hohenheim, 2018.
13. Wagner, G.; Behrendt, A.; Wulfmeyer, V.; Späth, F.; Schiller, M. High-power Ti:sapphire laser at 820 nm for scanning ground-based water vapor differential absorption lidar. *Appl. Opt.* **2013**, *52*, 2454–2469. doi:10.1364/AO.52.002454.
14. Hannemann, S.; van Duijn, E.J.; Ubachs, W. A narrow-band injection-seeded pulsed titanium:sapphire oscillator-amplifier system with on-line chirp analysis for high-resolution spectroscopy. *Review of Scientific Instruments* **2007**, *78*, 103102. doi:10.1063/1.2789690.
15. Zheng, J.; Katsuragawa, M. Freely designable optical frequency conversion in Raman-resonant four-wave-mixing process. *Scientific Reports* **2015**, *5*, 8874. doi:10.1038/srep08874.
16. Chemnitz, M.; Baumgartl, M.; Meyer, T.; Jauregui, C.; Dietzek, B.; Popp, J.; Limpert, J.; Tünnermann, A. Widely tuneable fiber optical parametric amplifier for coherent anti-Stokes Raman scattering microscopy. *Opt. Express* **2012**, *20*, 26583–26595. doi:10.1364/OE.20.026583.
17. Lefrancois, S.; Fu, D.; Holtom, G.R.; Kong, L.; Wadsworth, W.J.; Schneider, P.; Herda, R.; Zach, A.; Xie, X.S.; Wise, F.W. Fiber four-wave mixing source for coherent anti-Stokes Raman scattering microscopy. *Opt. Lett.* **2012**, *37*, 1652–1654. doi:10.1364/OL.37.001652.
18. Thariyan, M.P.; Bhuiyan, A.H.; Meyer, S.E.; Naik, S.V.; Gore, J.P.; Lucht, R.P. Dual-pump coherent anti-Stokes Raman scattering system for temperature and species measurements in an optically accessible high-pressure gas turbine combustor facility. *Measurement Science and Technology* **2010**, *22*, 015301. doi:10.1088/0957-0233/22/1/015301.
19. Hamilton, C.E. Single-frequency, injection-seeded Ti:sapphire ring laser with high temporal precision. *Opt. Lett.* **1992**, *17*, 728–730. doi:10.1364/OL.17.000728.
20. Drever, R.W.P.; Hall, J.L.; Kowalski, F.V.; Hough, J.; Ford, G.M.; Munley, A.J.; Ward, H. Laser phase and frequency stabilization using an optical resonator. *Applied Physics B* **1983**, *31*, 97–105. doi:10.1007/BF00702605.
21. Tomita, H.; Mattolat, C.; Kessler, T.; Raeder, S.; Schwellnus, F.; Wendt, K.; Watanabe, K.; Iguichi, T. Ultra Trace Determination Scheme for 26 Al by High-Resolution Resonance Ionization Mass Spectrometry using a Pulsed Ti:Sapphire Laser. *Journal of Nuclear Science and Technology* **2008**, *45*, 37–42. doi:10.1080/00223131.2008.10875974.
22. Henderson, S.W.; Yuen, E.H.; Fry, E.S. Fast resonance-detection technique for single-frequency operation of injection-seeded Nd:YAG lasers. *Opt. Lett.* **1986**, *11*, 715–717. doi:10.1364/OL.11.000715.
23. Walther, T.; Larsen, M.P.; Fry, E.S. Generation of Fourier-transform-limited 35-ns pulses with a ramp-hold-fire seeding technique in a Ti:sapphire laser. *Appl. Opt.* **2001**, *40*, 3046–3050. doi:10.1364/AO.40.003046.
24. Raymond, T.; Smith, A. Two-frequency injection-seeded Nd:YAG laser. *IEEE Journal of Quantum Electronics* **1995**, *31*, 1734–1737. doi:10.1109/3.466046.

25. Tamura, K. Properties of a Pulsed Ti:Sapphire Laser Oscillator with an Extended Standing-Wave Cavity. *Journal of Nuclear Science and Technology* **2009**, *46*, 316–319. doi:10.1080/18811248.2007.9711536.
26. Suzuki, H.; Kuribayashi, O.; Kannari, F. Synchronous dual-wavelength operation of a self-injection-seeded narrow-linewidth flash-lamp-pumped Q-switched Ti:Al2O3 laser. *Opt. Lett.* **1997**, *22*, 1710–1712. doi:10.1364/OL.22.001710.
27. Li, R.; Lassen, J.; Rothe, S.; Teigelhöfer, A.; Mostamand, M. Continuously tunable pulsed Ti:Sa laser self-seeded by an extended grating cavity. *Opt. Express* **2017**, *25*, 1123–1130. doi:10.1364/OE.25.001123.
28. Barnes, N.; Williams, J.; Barnes, J.; Lockard, G. A self-injection locked, Q-switched, line-narrowed Ti:Al_2O_3 laser. *IEEE Journal of Quantum Electronics* **1988**, *24*, 1021–1028. doi:10.1109/3.224.
29. Tamura, K. Single-longitudinal-mode scan of a pulsed double-grating Ti:sapphire oscillator. *Appl. Opt.* **2007**, *46*, 5924–5927. doi:10.1364/AO.46.005924.
30. Raymond, T.D.; Esherick, P.; Smith, A.V. Widely tunable single-longitudinal-mode pulsed dye laser. *Opt. Lett.* **1989**, *14*, 1116–1118. doi:10.1364/OL.14.001116.
31. Binks, D.J.; Gloster, L.A.W.; King, T.A.; McKinnie, I.T. Frequency locking of a pulsed single-longitudinal-mode laser in a coupled-cavity resonator. *Appl. Opt.* **1997**, *36*, 9371–9377. doi:10.1364/AO.36.009371.
32. Crawford, T.; Lowrie, C.; Thompson, J.R. Prelase stabilization of the polarization state and frequency of a Q-switched, diode-pumped, Nd:YAG laser. *Appl. Opt.* **1996**, *35*, 5861–5869. doi:10.1364/AO.35.005861.
33. Dai, W.; Jin, L.; Dong, Y.; Jin, G. Experimental Investigation of a High-repetition-rate Pr3+:YLF Laser with Single-frequency Oscillation. *Current Optics and Photonics* **2021**, *5(6)*, 721–729. doi:10.3807/COPP.2021.5.6.721.
34. Qing-Song, L.; Yuan, D.; Yu, L.; Xi-He, Z.; Yong-Ji, Y.; Guang-Yong, J. Effect of cavity length on low-energy single longitudinal mode pre-lase Q-switched laser. *Optics & Laser Technology* **2017**, *94*, 165–170. doi:https://doi.org/10.1016/j.optlastec.2017.03.033.
35. Backus, S.; Kirchner, M.; Durfee, C.; Murnane, M.; Kapteyn, H. Direct diode-pumped Kerr Lens 13 fs Ti:sapphire ultrafast oscillator using a single blue laser diode. *Opt. Express* **2017**, *25*, 12469–12477. doi:10.1364/OE.25.012469.
36. Song, D.H.; Seo, H.S. Spectrally combined three-diode-pumped compact femtosecond Ti:sapphire laser exceeding 1 W mode-locked power. *Opt. Express* **2021**, *29*, 32649–32657. doi:10.1364/OE.438230.
37. Durfee, C.G.; Storz, T.; Garlick, J.; Hill, S.; Squier, J.A.; Kirchner, M.; Taft, G.; Shea, K.; Kapteyn, H.; Murnane, M.; et al. Direct diode-pumped Kerr-lens mode-locked Ti:sapphire laser. *Opt. Express* **2012**, *20*, 13677–13683. doi:10.1364/OE.20.013677.
38. Rohrbacher, A.; Olarte, O.E.; Villamaina, V.; Loza-Alvarez, P.; Resan, B. Multiphoton imaging with blue-diode-pumped SESAM-modelocked Ti:sapphire oscillator generating 5 nJ 82 fs pulses. *Opt. Express* **2017**, *25*, 10677–10684. doi:10.1364/OE.25.010677.
39. Liu, H.; Sun, S.; Zheng, L.; Wang, G.; Tian, W.; Zhang, D.; Han, H.; Zhu, J.; Wei, Z. Review of laser-diode pumped Ti:sapphire laser. *Microwave and Optical Technology Letters* **2021**, *63*, 2135–2144. doi:10.1002/mop.32882.
40. Miao, Z.W.; Yu, H.J.; Zou, S.Z.; He, C.J.; Zhao, P.F.; Lou, B.J.; Lin, X.C. Low-threshold-intensity 3.8-W continuous-wave Ti:Sapphire oscillator directly pumped with green diodes. *Applied Physics B* **2021**, *127*, 105. doi:10.1007/s00340-021-07652-3.
41. Roth, P.W.; Burns, D.; Kemp, A.J. Power scaling of a directly diode-laser-pumped Ti:sapphire laser. *Opt. Express* **2012**, *20*, 20629–20634. doi:10.1364/OE.20.020629.
42. Backus, S.; Kirchner, M.; Lemons, R.; Schmidt, D.; Durfee, C.; Murnane, M.; Kapteyn, H. Direct diode pumped Ti:sapphire ultrafast regenerative amplifier system. *Opt. Express* **2017**, *25*, 3666–3674. doi:10.1364/OE.25.003666.
43. Sonnenschein, V.; Tomita, H.; Kotaro, K.; Koya, H.; Studer, D.; Terabayashi, R.; Weber, F.; Wendt, K.; Nishizawa, N.; Iguchi, T. A direct diode pumped Ti:sapphire laser with single-frequency operation for high resolution spectroscopy. *Hyperfine Interactions* **2020**, *241*, 32. doi:10.1007/s10751-020-1706-4.
44. Sonnenschein, V.; Ohashi, M.; Tomita, H.; Iguchi, T. A direct diode pumped continuous-wave Ti:sapphire laser as seed of a pulsed amplifier for high-resolution resonance ionization spectroscopy. *Nuclear Instruments and Methods in Physics Research Section B: Beam Interactions with Materials and Atoms* **2020**, *463*, 512–514. doi:10.1016/j.nimb.2019.03.017.
45. Jin, P.; Lu, H.; Wei, Y.; Su, J.; Peng, K. Single-frequency CW Ti:sapphire laser with intensity noise manipulation and continuous frequency-tuning. *Opt. Lett.* **2017**, *42*, 143–146. doi:10.1364/OL.42.000143.
46. Gong, Q.; Zhao, C.; Yang, Y.; Fang, Q.; Li, S.; Xu, M.; Hang, Y. Theoretical study on residual infrared absorption of Ti:sapphire laser crystals. *Photon. Res.* **2021**, *9*, 909–915. doi:10.1364/PRJ.418395.
47. Moulton, P.F.; Cederberg, J.G.; Stevens, K.T.; Foundos, G.; Koselja, M.; Preclikova, J. Optimized InGaN-diode pumping of Ti:sapphire crystals. *Opt. Mater. Express* **2019**, *9*, 2131–2146. doi:10.1364/OME.9.002131.
48. Zhou, W.; Mori, Y.; Sasaki, T.; Nakai, S.; Nakano, K.; Niikura, S.; Craig, B. Intracavity frequency doubling of a continuous wave Ti:sapphire laser with over 70% conversion efficiency. *Applied Physics Letters* **1995**, *66*, 2463–2465. doi:10.1063/1.113996.
49. Cruz, L.S.; Cruz, F.C. External power-enhancement cavity versus intracavity frequency doubling of Ti:sapphire lasers using BIBO. *Opt. Express* **2007**, *15*, 11913–11921. doi:10.1364/OE.15.011913.
50. Sonnenschein, V.; Moore, I.D.; Pohjalainen, I.; Reponen, M.; Rothe, S.; Wendt, K., Intracavity Frequency Doubling and Difference Frequency Mixing for Pulsed ns Ti:Sapphire Laser Systems at On-Line Radioactive Ion Beam Facilities. In *Proceedings of the Conference on Advances in Radioactive Isotope Science (ARIS2014)*; The Physical Society of Japan, 2014; pp. 030126–1–030126–6. doi:10.7566/JPSCP.6.030126.